Optical, mechanical and fractographic response of transparent alumina ceramics on erbium doping

DRDLÍK, D.; DRDLÍKOVÁ, K.; HADRABA, H.; MACA, K.

Analog Integrated Circuits and Signal Processing
2017, vol. 37, iss. 14, pp. 4265-4270

ISSN: 0955-2219

DOI: http://dx.doi.org/10.1016/j.jeurceramsoc.2017.02.043

Accepted manuscript

Optical, mechanical and fractographic response of transparent alumina ceramics on erbium doping

Daniel Drdlik[a], Katarina Drdlikova[a], Hynek Hadraba[b] and Karel Maca[a]

[a] *CEITEC BUT, Brno University of Technology, Purkynova 123, 612 00 Brno, Czech Republic*

[b] *CEITEC IPM, Institute of Physics of Materials, Academy of Sciences of the Czech Republic, Zizkova 513/22, 616 62 Brno, Czech Republic*

Abstract

Alumina ceramics found their utilisation in many applications which can be further extend by attaining functional properties; in our case the transparency obtained through precise processing and photoluminescence due to erbium (Er) doping. In order to examine the optical, mechanical and fractographic response of transparent alumina on Er doping, slip casted samples containing 0 - 0.15 at.% of erbium nano-oxide were pre-sintered by two-step sintering regime and then hot isostatically pressed. Prepared samples exhibited fully dense submicron microstructure and corresponding high transparency (RIT up to 60%). Positive influence of doping on the Vickers hardness resulted in values up to 27 GPa (at 10N load). Moreover, the comparison of the Vickers hardness determined at different loadings with literature data showed that the Er doped alumina is one of the hardest material in this category. The samples were characterised also in terms of fracture toughness and fractographic behaviour.

Keywords

Alumina; erbia; transparency, hardness; fractography

1. Introduction

Polycrystalline alumina is the most widely used structural ceramics in many common applications. When the alumina has extremely fine microstructure (low grain size) without residual porosity (final density ≥ 99.95%) then it becomes transparent [1]. Transparent polycrystalline alumina has a great technological potential for highly demanding applications which take advantage of its superior mechanical properties like high hardness, wear resistance, and high strength, in addition to its optical performance in the infrared and visible domain [2]. Moreover, in relation to the post-machining costs and inferior mechanical properties of sapphire (single crystal of alumina) the fine polycrystalline alumina exhibits economic and ecological benefits [3]. Krell et al. suggested application potential of this material in several directions: i) lighting, ii) optical components for different wavelengths, iii) infrared emitters, iv) orthodontic appliances and v) ceramic armours [1, 4].

To ensure transparency of the alumina few processing conditions must be fulfilled. The alumina powder should be extremely pure (99.99%) with nearly nanometre particle size and the grain growth during sintering has to be limited. The authors mainly utilise advantage of short sintering times using spark plasma sintering (SPS) [5-7]. However, to ensure other optical performances, i.e. photoluminescence, the doping with e.g. rare earth (RE) elements is needed [8-10]. By doping with the aim to obtain another functional property, it must be taken into account that the addition of sufficient amount of dopant can lead to the transparency deterioration. On the other hand, through the doping the alumina obtains interesting optical properties and pinning effect of dopant allows keeping low grain size. As doping elements for microstructure optimisation there are commonly used metals as chromium [11], titanium [12], magnesium [12-14], zirconium [15], or rare earth metals as yttrium [13], lanthanum [13]. Less common is doping with terbium [8], cerium [16], europium [9] or erbium [17, 18].

Generally, mechanical properties and fractographic analysis of the transparent and/or photoluminiscent alumina is not well described in literature; only few publications on this topic can be found in the relevant literature. Krell et al. [19] doped commercial corundum powder with 0.03 wt.% MgO and 0.2 wt.% ZrO_2. In this transparent material no evidence of spinel phase and hardness 20–21 GPa (HV10) were obtained. The same combination of dopants used Braun et al. [20] to prepare transparent polycrystalline alumina with sub-micrometre microstructure. They studied the influence of different MgO and ZrO_2 dopant levels on the densification, microstructure development and in-line transmittance values. Nevertheless, authors provided information about hardness measurement valid only for undoped transparent alumina samples. The reported hardness ~11.6 GPa was relatively low probably due to higher value of grain size. In case of alumina doping with the rare earth elements Biswas et al. [3] reported hardness 21.4 GPa (HV5) of transparent sub-micrometre alumina doped with 0.1 wt.% lanthanum oxide.

Due to the lack of literature data this work is focused on investigation of optical, mechanical and fracture properties of transparent and/or photoluminescent alumina doped with various amount of erbia. Hardness measurement of alumina samples is extended to various load forces in order to enable better discussion with literature. Both hardness and fracture toughness are related to the observed microstructure. To the best of our knowledge, no similar study was carried out on this type of transparent and photoluminiscent material before.

2. Experimental

The commercial alumina powder (TM-DAR, Taimei Chemicals Co., Japan) with average particle size of 150 nm and commercial erbia powder (GNM, Getnanomaterials, USA) with average particle size of 20-30 nm were used for preparation of stable suspensions. Suspensions contain 45 vol.% of alumina, certain amount of erbia dopant (0, 0.10, 0.11, 0.125 and 0.15 at.%), electrostatic stabilizer (Darvan CN, Vanderbilt Minerals, USA) and deionized water. To remove aggregates the erbia powder was centrifugated at 800 rpm for 2 min before adding into suspension. Suspensions were homogenized for 24 hours in a plastic bottles filled by alumina milling balls with diameter 4 mm. The balls to powder milling ratio of 2:1 was used.

The homogenous suspensions were casted into PVC dishes. Erbia doped alumina discs with diameter approximately 50 mm were first dried at room temperature for three days and then at 80°C for 5 h. The discs were pressureless pre-sintered up to closed porosity stage (density range 95-96% [18, 21] using two-step sintering (TSS) in ambient atmosphere. The first step of TSS was realized at 1440°C without dwell time followed by the cooling (20°C/min) to the temperature 1280°C with dwell time 10 h. The amount of open pores was checked by means of Archimedes method (EN 623-2). The two-step pre-sintered samples were consequently hot isostatically pressed under 200 MPa pressure of argon atmosphere at 1280°C to completely eliminate residual closed porosity.

Sintered discs were grinded and polished up to 1 μm surface roughness, final thickness of the discs was approximately 0.8 mm. The real in-line transmittance (RIT) of the samples was measured with a non-polarized He-Ne laser (λ=632.8 nm) at 860 mm sample to detector distance and 0.5° opening angle. The samples were thermally etched and investigated using a Lyra 3 microscope (Tescan, Czech Republic) and Titan Themis 60-300 (FEI, Czech Republic) equipped by Quantax EDX (Bruker Nano, Germany). During this investigation at least 5

micrographs of microstructure were obtained. The mean grain size (MGS) was determined on each micrograph using linear intercept method. The final average grain size value was multiplied by correction factor 1.56 [22].

Hardness was measured using an instrumented hardness tester (Z2.5, Zwick/Roel, Germany) at loading from 1 to 100 N. The number of measurements for each sample was set to 15. The fracture toughness was calculated from the length of the cracks originating from the corners of the indentation using equation [23]:

$$K_c = \propto \sqrt{\frac{E}{H}} \frac{P}{c^{3/2}}, \qquad (1)$$

where α is an empirically determined constant (0.016), E is Young's modulus, H is the hardness, P is the applied load and c is the length of the crack grown from indent corner. Length of indent diagonals and cracks were measured using confocal microscope LEXT OLS 3100 (Olympus, Japan).

3. Results and discussion

Processing of the RE-doped transparent alumina was described in our previous work [18]. In the present work, one undoped and four Er^{3+}-doped transparent alumina discs were prepared. The photograph of transparent alumina discs doped by Er^{3+} in concentrations of 0.10, 0.11, 0.125 and 0.15 at.% is shown in Fig. 1. The samples were placed 5 mm above the printed paper. It is evident that transparency is similar for all samples. The real in-line transmittance of doped samples was in range 53-56% whereas the real in-line transmittance of undoped alumina was slightly higher (60%). Summary of RIT values is given in Table 1. The obtained RIT values were also recalculated to 1 mm thickness and related to the maximum theoretical transparency value for alumina (86% at 840 nm) for easier comparison with literature data [24]. The RIT of Er^{3+}-doped alumina in the range of 53-59% was already established in our previous work [18]. Here it was compared with RIT of undoped alumina prepared by the same way. The lower RIT value of doped alumina was expected because the relative high concentration of the dopant probably exceeded the amount being able to the segregate at the grain boundaries (e.g. lanthanum grain boundary solubility limit in alumina was observed at ~200 ppm [25]). Therefore, the higher content of the dopant then most likely results in decrease of optical transmittance.

Only few works reported optical transparency of photo- or thermoluminiscent alumina doped by Tb [8], Eu [9] and Ce [16]. In those cases the obtained transparencies were low, suffering from inclusions present as a result of high dopant concentration and the samples were rather translucent than transparent.

It is well known that transparency of the transparent ceramics is grain size dependent. However, the MGS of prepared Er^{3+}-doped transparent alumina exhibited no trend; the MGS was in narrow range of 0.33-0.35 μm (see Table 1) irrespective of dopant concentration. The slightly

higher MGS of undoped alumina (0.50 μm) prepared at the same processing route confirmed grain growth inhibition (reduced mobility of grain boundaries) due to erbium presence at the grain boundaries. The segregation of Er^{3+} cations on the grain boundary was determined by EDX line scan. The EDX line scan of Al, O and Er elements through the grain boundary of Er^{3+}-doped alumina (0.10 at.% of Er^{3+}) with TEM detail of microstructure is showed in Fig. 2. The EDX line scan marked by pink arrow in detailed TEM micrographs of microstructure proved the presence of Er^{3+} cations on the grain boundary. The count of Er signal increased in this place (diamonds line) whereas signal of Al and O (circles and squares lines) atoms slightly decreased. This situation confirmed that the amount of dopant was higher than the bulk solubility limit (solubility in alumina is very low ~10^{-3} at.% [26]) and the segregation of Er occurs on grain boundaries. Taking into account the observed values of grain boundary solubility for La and Zr for similar alumina microstructures, the amount of added Er very likely exceeded the grain solubility limit and the secondary phases should appear at grain boundaries and triple points [25]. Nevertheless, no secondary phases were observed during SEM and TEM investigation, which may suggest different (much higher) value of grain boundary solubility limit for Er or the situation where very homogeneous distribution of the dopant results in very small, barely perceptible inclusions.

The Vickers hardness (at testing load of 10N) of the transparent alumina samples with different Er^{3+} concentration is shown in Fig. 3. From the hardness of undoped alumina (26.1 GPa), it is obvious that the high hardness of all samples is primarily related to the optimised processing (fine powders → optimised slip casting → TSS → HIP) leading to improved microstructure rather than possible hardening effect of erbia (which is anyway present in very small concentrations). The average hardness of Er^{3+}-doped transparent alumina samples (26.9 GPa) is slightly higher than undoped one. The hardness of the doped alumina samples varied only in the interval ±0.18 GPa. The improvement of the hardness due to erbia doping observed also

Joshi et al. [27]. They reported 2% increase in the hardness of erbia doped polycrystalline silicon nitride in comparison with undoped silicon nitride. This result is in good agreement with our 3% increase of the hardness. Generally, the hardness of ceramics is dependent on its porosity and grain size [28, 29]. However, the transparent ceramics contain porosity close to zero, so the main parameter influencing its hardness is the grain size. The slight increase of the hardness Er^{3+}-doped transparent aluminas in contrast to undoped alumina corresponds also with the Hall-Petch relationship where the hardness increases with the smaller grains [30]. The second reason of the hardness improvement in Er^{3+}-doped transparent alumina could be solute solution strengthening mechanism [31]. However, this mechanism is probably less of importance.

Krell [32, 33] pointed out that hardness of polycrystalline alumina strongly depends on the indentation size (load), grain size and surface preparation. Neglecting of these conditions lead to the distortion of presented final hardness, especially in comparison with literature data. In our case both grain size (see Table 1) and surface preparation were constant. Therefore, only one sample of transparent alumina doped by 0.15 at.% of Er^{3+} was selected for Vickers hardness measurements at different loads. The dependence of hardness of Er^{3+}-doped alumina on the different indentation force is shown in Fig. 4. Our results (green circles) are compared with other authors who worked with polycrystalline (mostly transparent) doped (red triangles) or undoped (blue squares) aluminas. It is obvious from this comparison that the hardness of prepared transparent Er^{3+}-doped alumina is very high; higher than the published literature data. However, it is important to note that only hardness reported in works [34-36] was measured in alumina samples with the similar or lower MGS. The MGS of alumina samples reported by other authors was in range 0.5-0.8 μm.

The fracture toughness of transparent and/or photoluminiscent alumina materials is not quite well discussed in literature. The indentation fracture toughness of Er^{3+}-doped alumina was in

range 2.1-2.2 MPa·$m^{1/2}$. The indentation fracture toughness of undoped alumina was slightly higher 2.3 MPa·$m^{1/2}$. These nearly the same fracture toughness values were expected because prepared ceramics contained uniform, equiaxed and fine grains [37]. On the other hand, it also indicates high strength [37]. The similar fracture toughness 2.9 and 3.2 MPa·$m^{1/2}$ at undoped and MgO doped alumina were reported in works Nishiyama et al. [36] and Shen et al. [7], respectively. Hesabi et al. [38] provided fracture toughness 4.2 MPa·$m^{1/2}$ and completely intergranular character of fracture surface of alumina sintered under optimised TSS regime. Nevertheless, their sample contained 2% porosity which could lead to reduction in the crack length by stopping and re-initiation of the crack growth on the pores.

The micrographs of fracture surfaces of undoped and Er^{3+}-doped alumina are shown in Fig. 5. The fractographic analysis showed a higher transgranular character of fracture surface in Er^{3+}-doped alumina compare to undoped alumina. The observed proportional fracture is in apparent contradiction with observations in work of West et al. [39] where detailed study of fracture surfaces of RE-doped (Yb, Gd, La) and undoped alumina with various MGS was provided. On the other hand, it should be note that there are a number of studies with different conclusions, e.g. Rani et al. [37] reported dominant transgranular fracture of pressureless sintered Er- and La-doped alumina. Nevertheless, our results reveal that Er dopant promotes the grain boundary cohesion.

The micrographs of cracks at the corners of Vickers indents of the undoped alumina and Er^{3+}-doped alumina (0.10 and 0.15 at.%) are shown in Fig. 6. The crack path in undoped alumina sample was not as straight as in the case of Er^{3+}-doped samples which proved predominant intergranular character of fracture and it may explain slight increase in the fracture toughness of undoped alumina in comparison with doped one.

4. Conclusion

The optical, microstructural, mechanical and fracture properties of Er^{3+}-doped transparent and/or photoluminescent alumina was investigated within this article. The real in-line transmittance (RIT) of Er^{3+}-doped samples was in range of 55-59% (recalculated to 1 mm thickness and related to the maximum theoretical transparency value for alumina), which belongs to higher RIT values in comparison with RITs found in literature. The presence of segregated Er atoms on the grain boundaries was proved by EDX line scan. Segregation of Er atoms on the grain boundary probably caused reduction of grain boundaries mobility which led to decreasing of the mean grain size (0.33-0.35 μm) in comparison to undoped alumina (0.50 μm). The Vickers hardness of the Er^{3+}-doped alumina was measured at different loading conditions and compared with literature. The current results indicates, that prepared transparent and/or photoluminescent Er^{3+}-doped alumina is one of the hardest material in this category, e.g. the Vickers hardness at 10 N loading was 26.9 GPa (average value for all Er^{3+} concentrations). The fractographic analysis showed a higher transgranular character of fracture surface in Er^{3+}-doped alumina compare to undoped alumina which confirms the enhanced grain boundary cohesion due to Er doping. The indentation fracture toughness of Er^{3+}-doped alumina was in range 2.1-2.2 $MPa \cdot m^{1/2}$. In conclusion, we reported here processing and properties of unique material with combination of superior optical, functional and mechanical properties.

Acknowledgements

This work is part of the project 5SA14857, which has acquired the financial contribution from the EU Framework Programme for Research and Innovation Horizon 2020 within the scope of the Marie Sklodowska-Curie Actions co-financed by the South Moravian Region according to the Grant Agreement no. 665860. The financial support of this work by the grant GACR 15-06390S is also gratefully acknowledged. This research has also been financially supported by the Ministry of Education, Youth and Sports of the Czech Republic under the project CEITEC 2020 (LQ1601). Part of the work was carried out with the support of core facilities of CEITEC open access project, ID number LM2011020, funded by the Ministry of Education, Youth and Sports of the Czech Republic under the activity „Projects of major infrastructures for research, development and innovations".

References

[1] A. Krell, J. Klimke, T. Hutzler, Advanced spinel and sub-mu m Al(2)O(3) for transparent armour applications, J Eur Ceram Soc 29(2) (2009) 275-281.

[2] A. Belenky, I. Bar-On, D. Rittel, Static and dynamic fracture of transparent nanograined alumina, J Mech Phys Solids 58(4) (2010) 484-501.

[3] P. Biswas, M.K. Kumar, K. Rajeswari, R. Johnson, U.S. Hareesh, Transparent sub-micrometre alumina from lanthanum oxide doped common grade alumina powder, Ceram Int 39(8) (2013) 9415-9419.

[4] A. Krell, T. Hutzler, J. Klimke, Transmission physics and consequences for materials selection, manufacturing, and applications, J Eur Ceram Soc 29(2) (2009) 207-221.

[5] L. Lallemant, G. Fantozzi, V. Garnier, G. Bonnefont, Transparent polycrystalline alumina obtained by SPS: Green bodies processing effect, J Eur Ceram Soc 32(11) (2012) 2909-2915.

[6] S. Grasso, H. Yoshida, H. Porwal, Y. Sakka, M. Reece, Highly transparent alpha-alumina obtained by low cost high pressure SPS, Ceram Int 39(3) (2013) 3243-3248.

[7] Z.J. Shen, M. Johnsson, Z. Zhao, M. Nygren, Spark plasma sintering of alumina, J Am Ceram Soc 85(8) (2002) 1921-1927.

[8] E.H. Penilla, Y. Kodera, J.E. Garay, Blue-Green Emission in Terbium-Doped Alumina (Tb:Al2O3) Transparent Ceramics, Adv Funct Mater 23(48) (2013) 6036-6043.

[9] Y. Yang, H. Wei, L.H. Zhang, K. Kisslinger, C.L. Melcher, Y.Q. Wu, Blue emission of Eu2+-doped translucent alumina, J Lumin 168 (2015) 297-303.

[10] X.J. Wang, M.K. Lei, T. Yang, H. Wang, Phase structure and photoluminescence Al2O3 powders prepared by the properties of Er3+-doped sol-gel method, Opt Mater 26(3) (2004) 247-252.

[11] Q. Liu, Q.H. Yang, G.G. Zhao, S.Z. Lu, H.J. Zhang, The thermoluminescence and optically stimulated luminescence properties of Cr-doped alpha alumina transparent ceramics, J Alloy Compd 579 (2013) 259-262.

[12] Q. Liu, Q.H. Yang, G.G. Zhao, S.Z. Lu, Titanium effect on the thermoluminescence and optically stimulated luminescence of Ti,Mg:alpha-Al2O3 transparent ceramics, J Alloy Compd 582 (2014) 754-758.

[13] M. Stuer, Z. Zhao, U. Aschauer, P. Bowen, Transparent polycrystalline alumina using spark plasma sintering: Effect of Mg, Y and La doping, J Eur Ceram Soc 30(6) (2010) 1335-1343.

[14] S. Chang, R.H. Doremus, L.S. Schadler, R.W. Siegel, Hot-pressing of nano-size alumina powder and the resulting mechanical properties, Int J Appl Ceram Tec 1(2) (2004) 172-179.

[15] M. Trunec, K. Maca, R. Chmelik, Polycrystalline alumina ceramics doped with nanoparticles for increased transparency, J Eur Ceram Soc 35(3) (2015) 1001-1009.

[16] I. Alvarez-Clemares, G. Mata-Osoro, A. Fernandez, S. Lopez-Esteban, C. Pecharroman, R. Torrecillas, J.S. Moya, Ceria doped alumina by Spark Plasma Sintering for optical applications, J Eur Ceram Soc 32(11) (2012) 2917-2924.

[17] T. Sanamyan, R. Pavlacka, G. Gilde, M. Dubinskii, Spectroscopic properties of Er3+-doped alpha-Al2O3, Opt Mater 35(5) (2013) 821-826.

[18] K. Bodisova, R. Klement, D. Galusek, V. Pouchly, D. Drdlik, K. Maca, Luminescent rare-earth-doped transparent alumina ceramics, J Eur Ceram Soc 36(12) (2016) 2975-2980.

[19] A. Krell, P. Blank, H.W. Ma, T. Hutzler, M.P.B. van Bruggen, R. Apetz, Transparent sintered corundum with high hardness and strength, J Am Ceram Soc 86(1) (2003) 12-18.

[20] A. Braun, G. Falk, R. Clasen, Transparent polycrystalline alumina ceramic with sub-micrometre microstructure by means of electrophoretic deposition, Materialwiss Werkst 37(4) (2006) 293-297.

[21] T. Spusta, J. Svoboda, K. Maca, Study of pore closure during pressure-less sintering of advanced oxide ceramics, Acta Mater 115 (2016) 347-353.

[22] M.I. Mendelson, Average Grain Size in Polycrystalline Ceramics, J Am Ceram Soc 52(8) (1969) 443-446.

[23] G.R. Anstis, P. Chantikul, B.R. Lawn, D.B. Marshall, A Critical-Evaluation of Indentation Techniques for Measuring Fracture-Toughness .1. Direct Crack Measurements, J Am Ceram Soc 64(9) (1981) 533-538.

[24] J. Petit, P. Dethare, A. Sergent, R. Marino, M.H. Ritti, S. Landais, J.L. Lunel, S. Trombert, Sintering of alpha-alumina for highly transparent ceramic applications, J Eur Ceram Soc 31(11) (2011) 1957-1963.

[25] L. Lallemant, N. Roussel, G. Fantozzi, V. Garnier, G. Bonnefont, T. Douillard, B. Durand, S. Guillemet-Fritsch, J.Y. Chane-Ching, D. Garcia-Gutierez, J. Aguilar-Garib, Effect of amount of doping agent on sintering, microstructure and optical properties of Zr- and La-doped alumina sintered by SPS, J Eur Ceram Soc 34(5) (2014) 1279-1288.

[26] M.D. Chambers, D.R. Clarke, Doped Oxides for High-Temperature Luminescence and Lifetime Thermometry, Annual Review of Materials Research 39(1) (2009) 325-359.

[27] B. Joshi, Z. Fu, K. Niihara, S.W. Lee, Optical, mechanical and tribological properties of Y 2 O 3 , Er 2 O 3 and Nd 2 O 3 doped polycrystalline silicon nitride ceramics, IOP Conference Series: Materials Science and Engineering 18(8) (2011) 082020.

[28] D. Drdlik, M. Slama, H. Hadraba, J. Cihlar, Hydroxyapatite/zirconia-microfibre composites with controlled microporosity and fracture properties prepared by electrophoretic deposition, Ceram Int 41(9) (2015) 11202-11212.

[29] R.W. Rice, C.C. Wu, F. Borchelt, Hardness Grain-Size Relations in Ceramics, J Am Ceram Soc 77(10) (1994) 2539-2553.

[30] C.S. Pande, K.P. Cooper, Nanomechanics of Hall-Petch relationship in nanocrystalline materials, Prog Mater Sci 54(6) (2009) 689-706.

[31] H.C. Ling, M.F. Yan, Microhardness Measurements on Dopant Modified Superconducting Yba2cu3o7 Ceramics, J Appl Phys 64(3) (1988) 1307-1311.

[32] A. Krell, A new look at the influences of load, grain size, and grain boundaries on the room temperature hardness of ceramics, Int J Refract Met H 16(4-6) (1998) 331-335.

[33] A. Krell, Improved hardness and hierarchic influences on wear in submicron sintered alumina, Mat Sci Eng a-Struct 209(1-2) (1996) 156-163.

[34] D. Chakravarty, G. Sundararajan, Effect of Applied Stress on IR transmission of Spark Plasma-Sintered Alumina, J Am Ceram Soc 93(4) (2010) 951-953.

[35] R.S. Mishra, C.E. Lesher, A.K. Mukherjee, High-pressure sintering of nanocrystalline gamma-Al2O3, J Am Ceram Soc 79(11) (1996) 2989-2992.

[36] N. Nishiyama, T. Taniguchi, H. Ohfuji, K. Yoshida, F. Wakai, B.N. Kim, H. Yoshida, Y. Higo, A. Holzheid, O. Beermann, T. Irifune, Y. Sakka, K. Funakoshi, Transparent nanocrystalline bulk alumina obtained at 7.7 GPa and 800 degrees C, Scripta Mater 69(5) (2013) 362-365.

[37] D.A. Rani, Y. Yoshizawa, K. Hirao, Y. Yamauchi, Effect of rare-earth dopants on mechanical properties of alumina, J Am Ceram Soc 87(2) (2004) 289-292.

[38] Z.R. Hesabi, A. Haghighatzadeh, M. Mazaheri, D. Galusek, S.K. Sadrnezhaad, Suppression of grain growth in sub-micrometer alumina via two-step sintering method, J Eur Ceram Soc 29(8) (2009) 1371-1377.

[39] G.D. West, J.M. Perkins, M.H. Lewis, The effect of rare earth dopants on grain boundary cohesion in alumina, J Eur Ceram Soc 27(4) (2007) 1913-1918.

[40] F.M. Liu, D.W. He, Q. Wang, W. Ding, J. Liu, Y.J. Liu, Bimodal transparent alumina ceramics prepared with micro/nano-particles under high pressure, Scripta Mater 122 (2016) 54-58.

Figure captions

Fig. 1 Transparent alumina discs doped by different Er^{3+} concentration at 5 mm distance over the printed paper.

Fig. 2 EDX line scan of Al, O and Er elements on the grain boundary of Er^{3+}-doped alumina (0.10 at.% of Er^{3+}) with TEM detail of microstructure.

Fig. 3 Vickers hardness (at testing load of 10N) of transparent alumina samples with different Er^{3+} concentration.

Fig. 4 Dependence of hardness of Er^{3+}-doped alumina (0.15 at.% of Er^{3+}) on the different indentation force.

Fig. 5 Fracture surface micrographs of a) undoped alumina sample and b) alumina samples doped by 0.15 at.% of Er^{3+}.

Fig. 6 Micrographs of cracks at the corners of Vickers indents of undoped alumina sample and alumina samples doped by 0.10 and 0.15 at.% of Er^{3+}.

Table captions

Table 1 Summary of microstructural and optical properties of undoped and Er^{3+}-doped alumina.

Table 1

Concentration of Er^{3+} (at.%)	Density (%)	MGS (μm)	RIT (%)	RIT_r* (%)
undoped		0.50	60	64
0.10		0.35	56	59
0.11	≥ 99.95	0.34	-	-
0.125		0.33	53	55
0.15		0.35	53	55

*RIT_r = RIT recalculated to 1 mm thickness and related to the maximum theoretical transparency value for alumina (86% at 840 nm).

Fig. 1

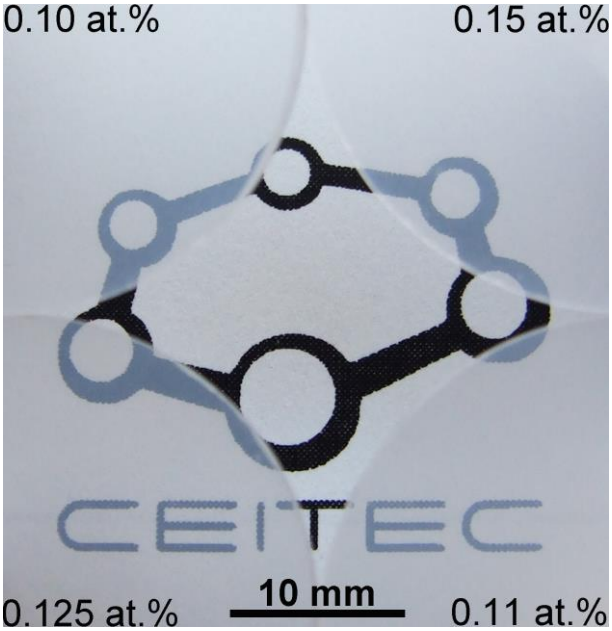

Fig. 2

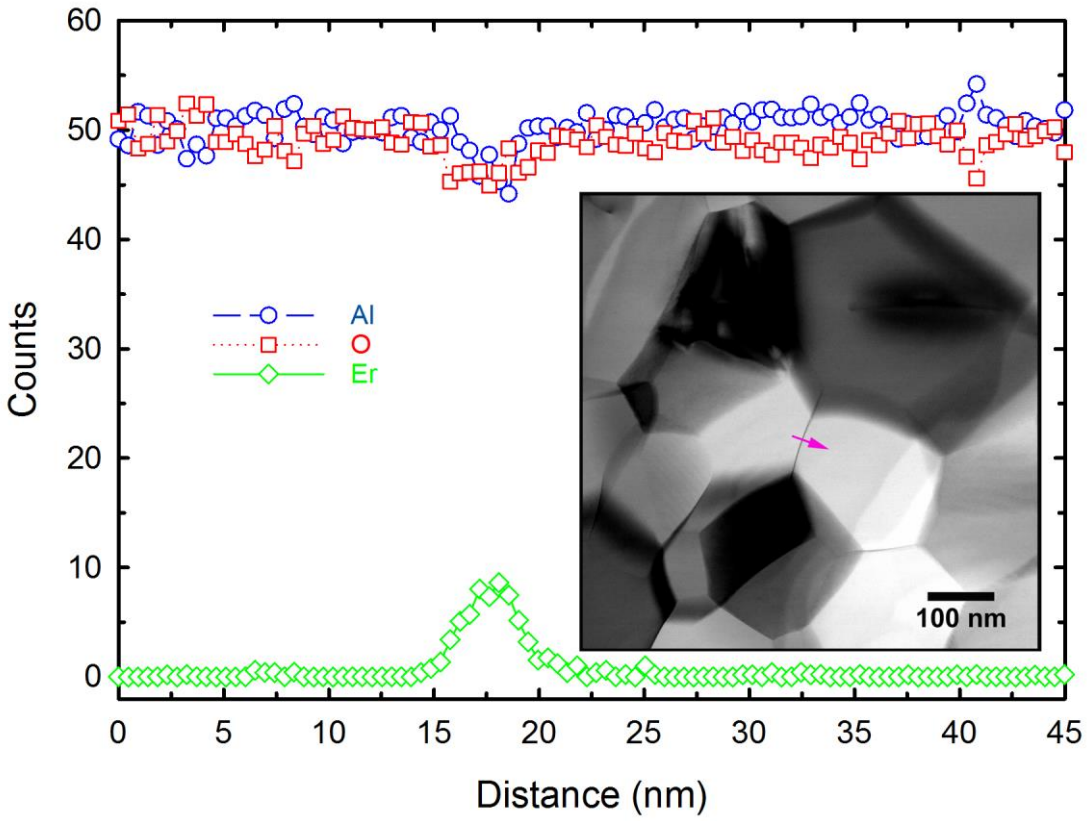
Counts
Distance (nm)
Al
O
Er
100 nm
0
10
20
30
40
50
60
0
5
10
15
20
25
30
35
40
45

Fig. 3

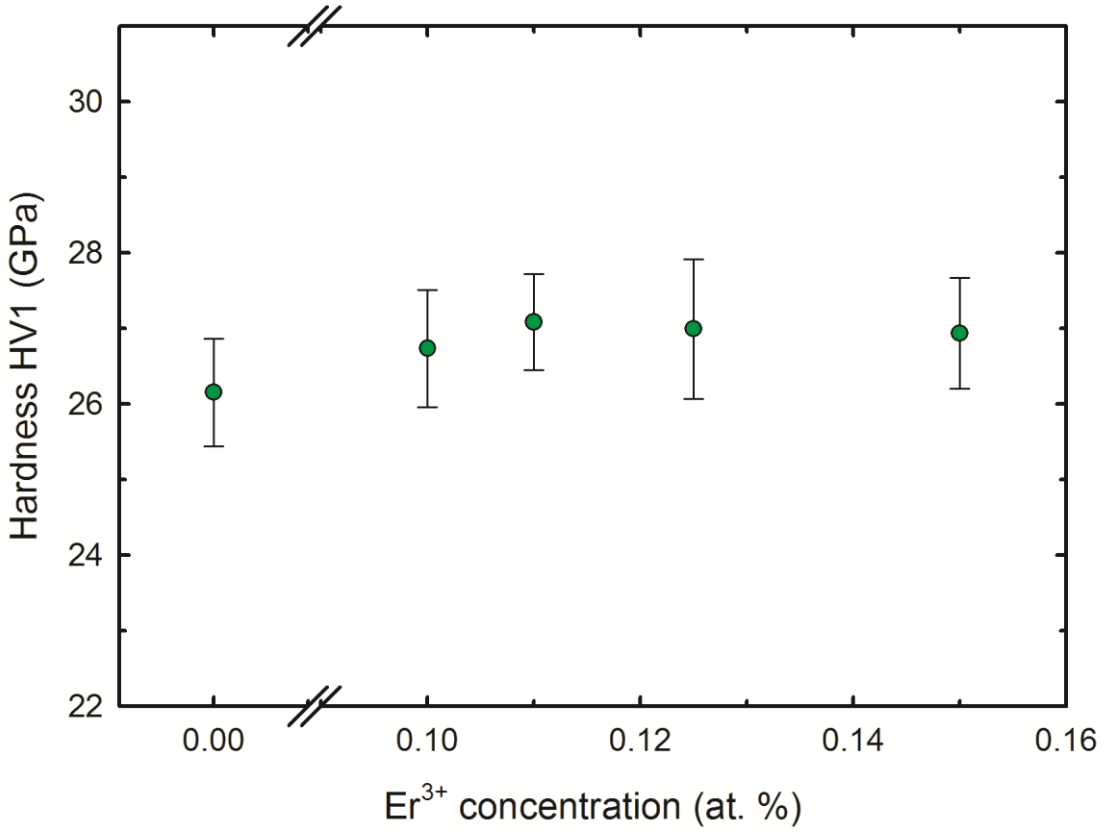
Hardness HV1 (GPa)
30
28
26
24
22
0.00
0.10
0.12
0.14
0.16
Er3+ concentration (at. %)

Fig. 4

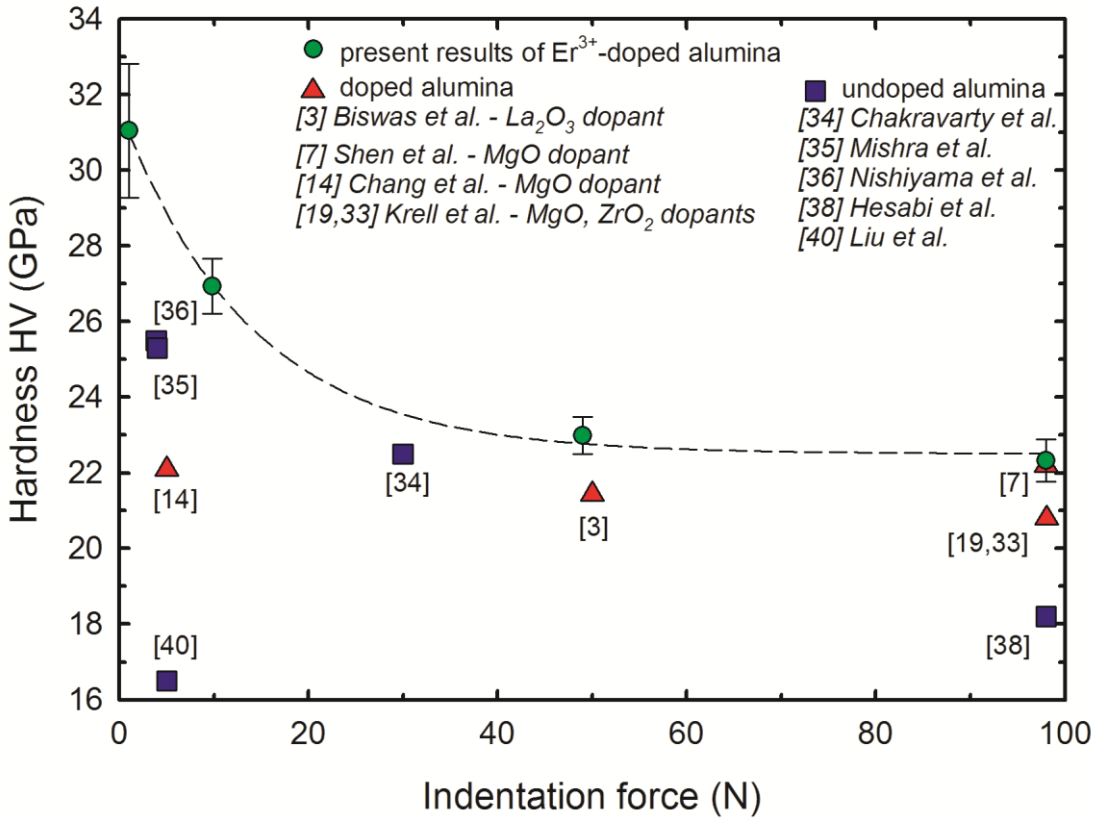
present results of Er3+-doped alumina
doped alumina
[3] Biswas et al. - La2O3 dopant
[7] Shen et al. - MgO dopant
[14] Chang et al. - MgO dopant
[19,33] Krell et al. - MgO, ZrO2 dopants
undoped alumina
[34] Chakravarty et al.
[35] Mishra et al.
[36] Nishiyama et al.
[38] Hesabi et al.
[40] Liu et al.
Hardness HV (GPa)
Indentation force (N)
34
32
30
28
26
24
22
20
18
16
0
20
40
60
80
100
[36]
[35]
[14]
[34]
[3]
[7]
[19,33]
[40]
[38]

Fig. 5

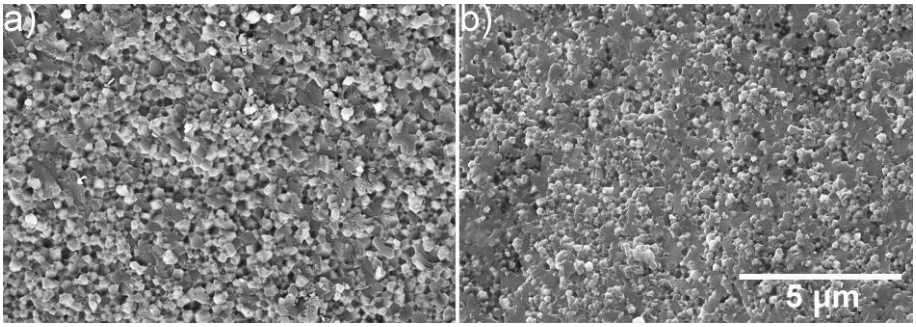

Fig. 6